

Figure S1 Thermotaxis behavior of *ttx-7(nj40);egl-8(nj77)* mutants (A) The neural circuit for thermotaxis behavior. Temperature information sensed by AFD and AWC sensory neurons is transmitted to AIY, AIZ and RIA interneurons. RIA neuron is assumed to integrate thermophilic drive conveyed from AIY neuron (designated as “T”) and cryophilic drive from AIZ neuron (designated as “C”) and to regulate downstream motor neurons. (B) Distributions and TTX indices of wild-type animals, *ttx-7(nj40)*, *ttx-7(nj40);egl-8(nj77)*, and *egl-8(nj77)* mutants cultivated at 17°, 20° and 23°. The marks on the bars

of each genotype indicate for comparisons with wild type. The marks on the lines represent for comparisons between indicated genotypes. Tukey–Kramer tests was performed ($n \geq 4$ assays). **(C)** RIA specific rescue experiments for *ttx-7(nj40);egl-8(nj77)* mutants cultivated at 23° using the population thermotaxis assay. Either the expression of *egl-8* cDNA or *egl-8* cDNA::*gfp* in RIA neuron of *ttx-7(nj40);egl-8(nj77)* mutants partially but significantly rescued the suppression of the thermotaxis defect. Tukey–Kramer test was performed ($n \geq 4$ assays). **(D)** Expressing *egl-8* cDNA specifically in RIA reduced the fraction of IT behavior in *ttx-7(nj40);egl-8(nj77)* double mutants. About 20 animals cultivated at 20° were examined in more than three trials, which were compared in ANOVA.

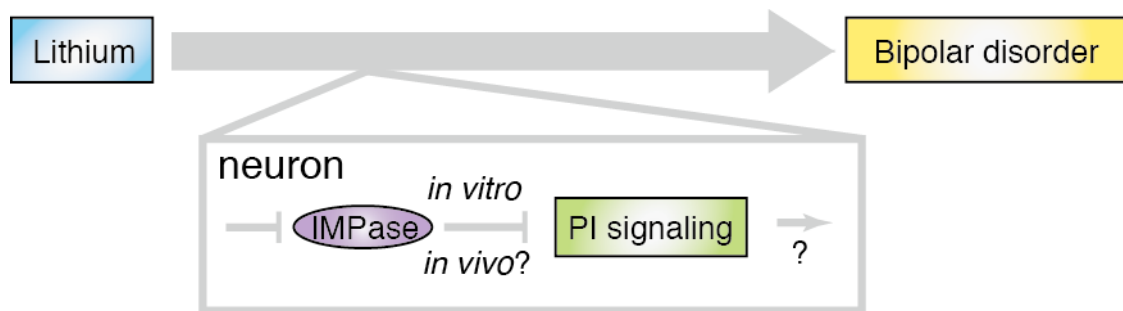


Figure S2 The inositol depletion hypothesis. The hypothesis explains that lithium exerts its effect on bipolar disorder via inhibition of IMPase. The inhibition of IMPase assumed to interfere with neuronal PI signaling but it has never been proven in vivo.

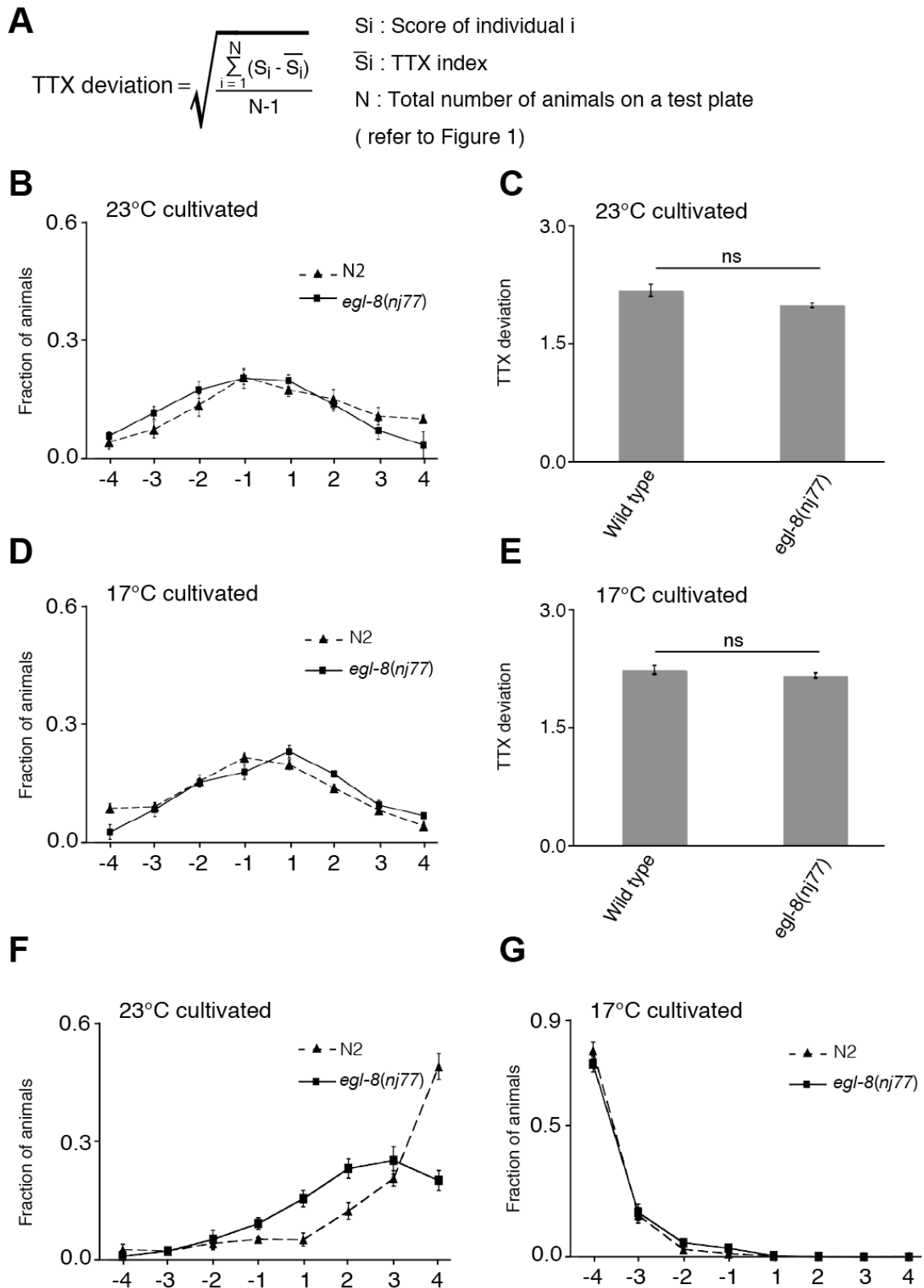


Figure S3 Thermotaxis behavior of *egl-8(nj77)* mutants. **(A)** The equation for calculating the TTX deviation. **(B and D)** Distributions of wild-type and *egl-8(nj77)* mutants on TTX plate without the temperature gradient ($n \geq 4$ assays). Animals cultivated at 23° **(B)** or 17° **(D)** were placed at the center of the plate and left for 60 min at 20°. **(C and E)** TTX deviations of

wild type and *egl-8(nj77)* mutants cultivated at 23° (C) and 17° (E). Although the TTX deviation of *egl-8* mutants was slightly lower than that of wild-type animals, the difference was not statistically significant. *t*-test was applied ($n \geq 4$ assays). **(F and G)** Animals cultivated at 23° (F) or 17° (G) were assayed in the population thermotaxis assay for 120 min ($n \geq 4$ assays). In contrast to the 60 min assay, *egl-8(nj77)* mutants cultivated at 17° migrated to the cultivation temperature as comparable to wild-type animals, but they did not at 23°.

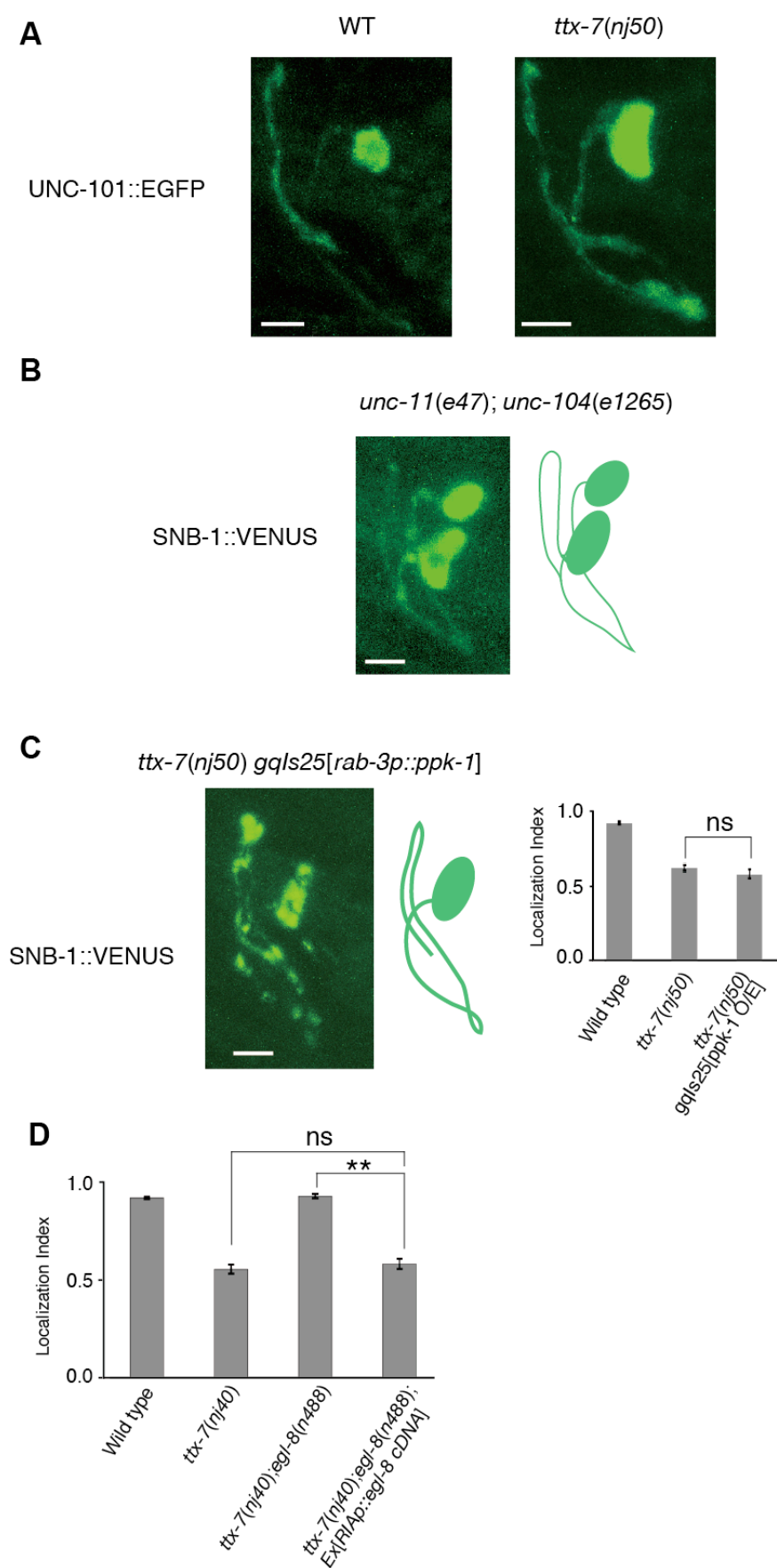


Figure S4 Localizations of synaptic components in RIA neuron. (A) The localization of UNC-101::GFP in RIA neuron. As described in Margeta et al. (2009), UNC-101::GFP was exclusively localized to the presynaptic region in wild-type animals. It

was mislocalized to the proximal region of the process in *ttx-7(nj50)* mutants. **(B)** The localization of SNB-1::VENUS in *unc-11(e47);unc-104(e1265)* double mutants. The fluorescence of SNB-1::VENUS was quite dim but observed in the entire process of RIA neuron. Scale bar, 5 μ m. **(C)** The representative image of the localization of SNB-1::VENUS in *ttx-7(nj50) gqls25[rab-3p::ppk-1]* mutants and the localization indices of SNB-1::VENUS in each genotype. The overexpression of *ppk-1* gene did not suppress the localization defect in *ttx-7* mutants. Steel-Dwass multiple comparison test was performed ($n \geq 8$ animals). Scale bar, 5 μ m. **(D)** RIA-specific expression of *egl-8* cDNA rescued the suppression of the SNB-1-localization defect by *egl-8(n488)* mutation. Steel-Dwass multiple comparison test was performed ($n \geq 15$ animals).